23rd International Congress on Sound & Vibration
Athens, Greece 10-14 July 2016
ICSV23

VIBRATION CONTROL OF BEAMS AND PLATES WITH HYBRID ACTIVE-PASSIVE CONSTRAINED LAYER DAMPING TREATMENTS

Byungjun Koh

Daewoo Shipbuilding and Marine Engineering, Noise & Vibration R&D Department, Seoul, 04521, South Korea
email: bkoh@dsme.co.kr

Emiliano Rustighi and Timothy Waters

University of Southampton, ISVR, Dynamics Group, Southampton, SO17 1BJ, UK

Brian Mace

University of Auckland, Department of Mechanical Engineering, Auckland, 1010, New Zealand

The concept of hybrid active-passive constrained layer damping treatments, which consists of viscoelastic materials, piezoelectric materials and elastic constraining materials, was proposed in the 1990s in order to ameliorate problems of instability in traditional active control systems in the higher frequency range. In this paper, the performances of four types of hybrid active-passive constrained layer damping treatments are investigated for beam and plate applications. These types are Active Constrained Layer Damping (ACLD), Active-Passive Constrained Layer Damping (APCLD), Active Control/Passive Constrained Layer Damping (AC/PCLD) and Active Control/Passive Stand-Off Layer Damping (AC/PSOLD). The performances of each treatment are compared through simulation with numerical models using the Finite Element Method. Finally, control performances of all configurations for curved plates are discussed with measured Frequency Response Functions of each case.

1. Introduction

In order to reduce the vibration of structures effectively, various methods such as Passive Constrained-Layer Damping (PCLD) and Active Control (AC) have been proposed and applied. However, as the need for application to various systems increased, these methods showed limits in performance due to their fundamental characteristics. For example, PCLD has a limited efficient range of application which depends on frequency and temperature. In particular, PCLD has very poor performances for low-frequency modes, and a significant increase of weight is needed to achieve appreciable vibration reduction. On the other hand, although AC can give good performance for low-frequency modes, instability problems can occur due to neglected high-frequency modes, and there are also robustness issues. To overcome the limits of each method, research has been carried out to combine PCLD and AC so as to have good performance at low and high frequencies at the same time [1, 2].

The first proposed configuration of this hybrid damping treatment was Active Constrained-Layer Damping (ACLD). In this case, the cover layer of PCLD was replaced by piezoelectric material. The basic concept was mentioned by Plump and Hubbard in 1986, but it was the publications by Baz in the early 1990s which allowed this method to gain wide-spread recognition [2]. In the two decades following Baz's research, various system configurations have been proposed with the aim of further

improving control performance [1, 2]. Recently, Trindade and Benjeddou [1] reviewed more than 80 papers regarding hybrid active-passive damping treatments using viscoelastic and piezoelectric materials, and categorised them into four types, which are shown in Figure 1. Active Passive Constrained-Layer Damping (APCLD) is a hybrid damping treatment where an additional elastic constraining layer is introduced to ACLD to enhance the stiffness of structure. For Active Control/Passive Constrained-Layer Damping (AC/PCLD), a PZT patch for active control is separate from the PCLD and can be located at different points according to control circumstances. In Active Control/Passive Stand-Off Layer Damping (AC/PSOLD), since the actuator elevates the PCLD, this leads to a PSOLD treatment in the open-loop case [1].

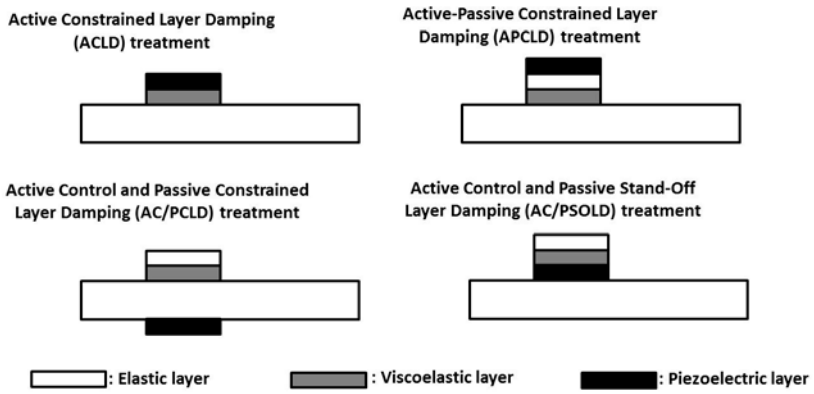

Figure 1: Four types of hybrid damping treatment described in [1]

Using FE models for cantilever beams, an impulsive transverse force and an iterative Linear Quadratic Regulator (LQR) control algorithm for the first three bending modes, Trindade and Benjeddou [1] compared control results using each configuration. They also changed the length of treatment and thickness of the viscoelastic layer. The optimal length of treatments and thickness of viscoelastic layers were investigated to obtain the greatest passive and active damping ratios. Moreover, the passive and active damping ratios of each type were found as functions of length and thickness. As a result, it was concluded that AC/PCLD and AC/PSOLD treatments can give more efficient results than other two methods. This was justified by the fact that in these two configurations the control force/moment could be delivered directly to the base beam without any loss which can happen in the viscoelastic layer with AC/PCLD and AC/PSOLD treatments. However, no closed-loop stability test was carried out. Also, these simulation results were not validated with experiments. Moreover, in [1], the results were for a particular beam with the treatment applied only at one location. There is also a need to investigate the generality of the finding in [1] regarding the base structure and the region treated. In this paper, these four types of hybrid damping are applied to beams. Experimental results are used to validate FE models to numerically investigate which treatment can give the most efficient control results.

In the next section, the experimental validation of the simulation results using measured frequency response functions (FRFs) will be presented. Then, the extension of application of the treatments to flat and curved plates and their control results follow. Finally, conclusions of this research and future works are discussed.

2. Control result verification for beams with measured FRFs

In order to verify the parameter study conclusion in [1], experimental samples were constructed using the configurations given in Figure 1. One example for ACLD treatment is shown in Figure 2. For other configurations, the treatments in red dotted circles were changed according to the order of lamination of each configuration. The dimensions of the aluminium base beams were 40 cm × 3 cm × 2.58 mm. Each treatment was composed of a PIC255 PZT patch (5 cm × 3 cm × 0.54 mm, d_{31}

direction polarisation, density: 7185.9 kg/m^3 by mass measurement), 3M viscoelastic damping polymer 112P05 (5 cm × 3 cm × 0.127 mm, density 1130 kg/m^3 from the manufacturer's data) and aluminium patch (5 cm × 3 cm × 0.36 mm, density 2249.7 kg/m^3 by mass measurement).

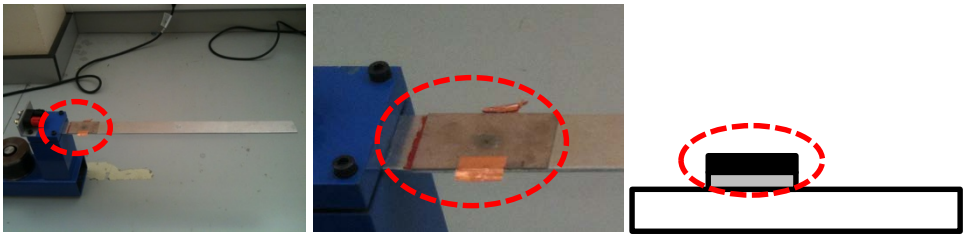

Figure 2: Experiment sample for ACLD treatment

For the experiment implementation, the block diagram of system control was set up as shown in Figure 3. In Figure 3, F_e, V_c, v_s and v_c denote the external primary disturbance, the control voltage, the velocity at the error sensing position and the controlled velocity at the point of interest, respectively. The control voltage can be determined by multiplying the control gain $-g$ and measured velocity at the error sensing position v_s. H^i_{jk} means the transfer function of case i between points j and k, where the superscript 'i' means the excitation by a shaker (denoted by f) or the excitation by a PZT actuator (denoted by v), and the subscripts 's', 'c' and 'e' mean the error sensing, the control and the excitation positions respectively. Therefore, if the transfer functions shown in Figure 3 can be obtained from experimental samples, the control performance of each configuration can be compared in the same condition.

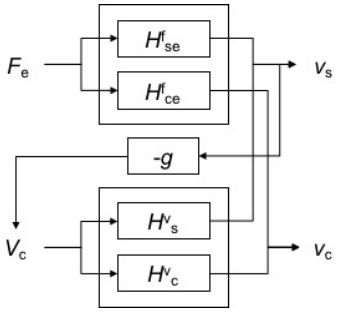

Figure 3: Block diagram of system control

In order to obtain the transfer functions of the system with the four configurations, experiments were conducted using the rig shown in Figure 4(a). In this system, the error sensing and the control points were set at the same point. Firstly, the transfer function $H^f_{se} = H^f_{ce}$ for shaker excitation was obtained with the set-up shown in Figure 4 (b). For the measurement of the transfer function $H^v_s = H^v_c$ for PZT patch excitation, the experimental set-up was realised as shown in Figure 4 (c). The transfer functions of the system in the block diagram in Figure 3 were measured for each configuration. As an example, the results of ACLD treatment are given in Figures 5 and 6 with the comparison of the transfer functions by numerical model based on FEM, as described in [3].

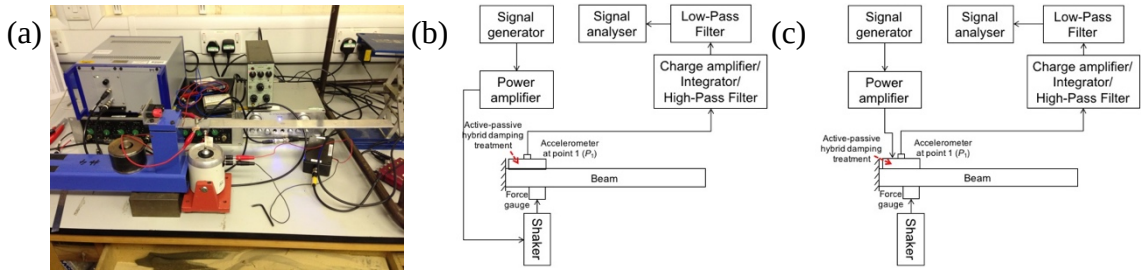

Figure 4: Experimental set-up for measurement; (a) real system, (b) schematic diagram for measurement of mobilities with shaker excitation (c) schematic diagram for measurement of FRFs of velocity per unit volt with electric pseudo-random excitation

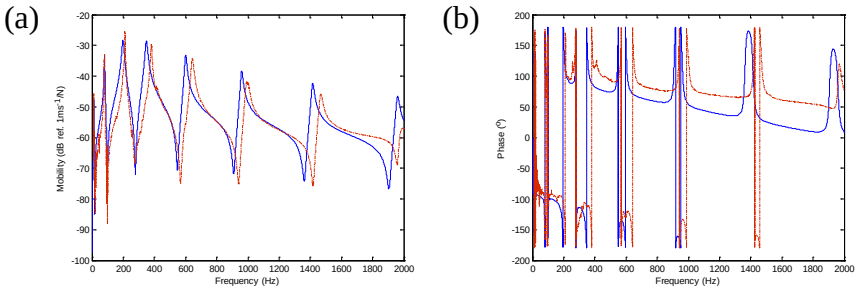

Figure 5: (a) Mobility $H^{f}_{se} = H^{f}_{ce}$ and (b) phases of Mobility $H^{f}_{se} = H^{f}_{ce}$ for a beam with ACLD treatment when a pseudo-random force is applied; ___ FE model and - - - measured data

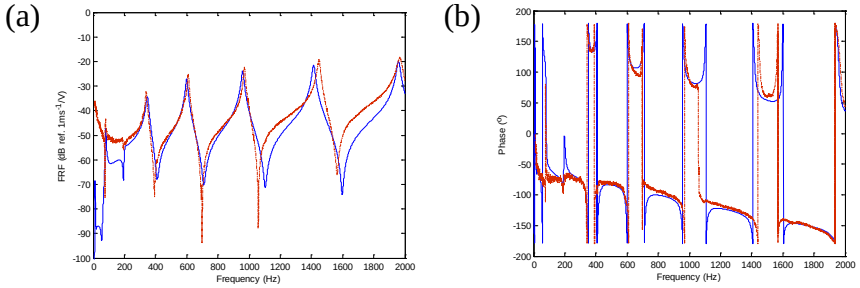

Figure 6: (a) FRFs of velocity per unit volt $H^{v}_{s} = H^{v}_{c}$ and (b) phases of velocity per unit volt $H^{v}_{s} = H^{v}_{c}$ for a beam with ACLD treatment when an electrical signal is applied to a PZT patch; ___ FE model and - - - measured data

Since the transfer function $H^{v}_{s} = H^{v}_{c}$ is equal to open loop control, the Nyquist plot of the open loop system can be found from the real and imaginary parts of $H^{v}_{s} = H^{v}_{c}$ for each configuration as shown in Figure 7. From the Nyquist plot of each configuration, control gains g which can guarantee the stability of control with 3 dB gain margin can be determined. Control signals were band limited to frequencies up to the first three resonances. With the determined control gains from the Nyquist plots, the reductions of mobility at the control point were obtained for each configuration as given in Figure 8.

As known from Figure 8, AC/PSOLD treatment can provide the largest reduction of vibration of the four HAPCLD treatments used. Contrary to the result in [1], the control result using AC/PCLD treatment was the worst of all. It is because of the reverse polarisation direction of the PZT patch used in this configuration. Considering the Nyquist plots in Figure 8 (c) and (d), AC/PCLD treatment is expected to give a similar result to AC/PSOLD treatment, but a smaller reduction.

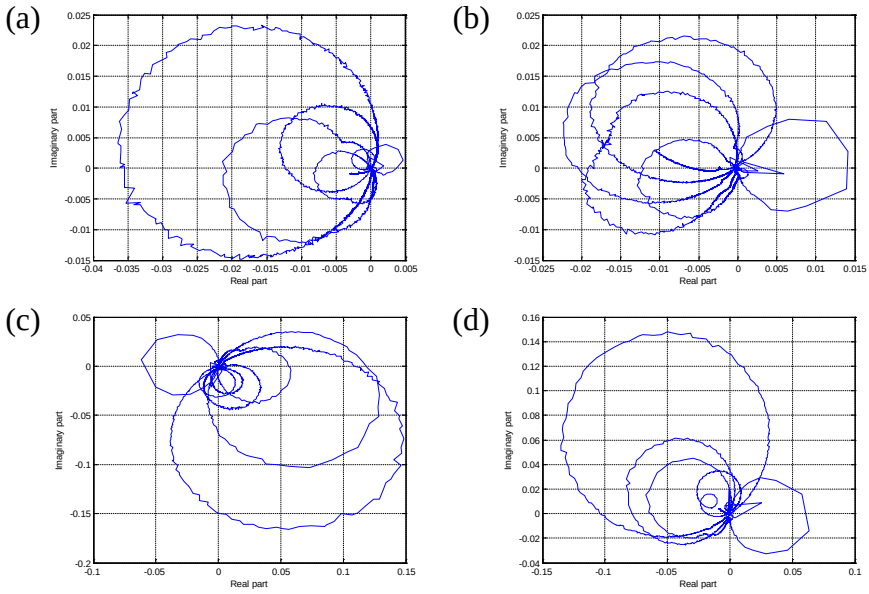

Figure 7: The Nyquist plots for the open loop of beam structures: (a) ACLD treatment, (b) APCLD treatment, (c) AC/PCLD treatment and (d) AC/PSOLD treatment

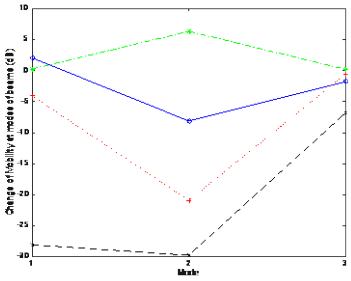

Figure 8: Change of Mobility by control of each HAPCLD treatment for beam; —— ACLD (g_{3dB}: 825.10), ------ APCLD (g_{3dB}: 1240), -·-·- AC/PCLD (g_{3dB}: 8.42) and – – AC/PSOLD (g_{3dB}: 1302)

3. Application to plates

As performed for beams, FE modelling method and application of HAPCLD treatments were applied to flat and curved plates [4]. The FE modelling of plates was established by extending the model of beams used in [3]. Additional Degree-of-Freedoms such as in-plane displacement and rotation about the *y*-direction, and a twisting term between *x*- and *y*-axes $\partial^2 w/\partial x \partial y$ were considered in the modelling in addition to the relations between in-plane displacements of each layer based on a layer-wise approach. The same method was applied to elastic, piezoelectric and viscoelastic materials. Shear deformation was considered only in the viscoelastic layer as was done for the beams. For curved plates, the coordinate changes at each node which should be considered between general flat FE plate elements and real curved plate elements according to curvatures were considered by introducing a coordinate transformation matrix. This coordinate transformation matrix for doubly curved plates was derived from the one for singly curved plates given in [5] as

$$\mathbf{T}_{\text{coord}} = \begin{bmatrix} \cos\varphi_{x_i} & -\sin\varphi_{x_i}\sin\varphi_{y_i} & -\sin\varphi_{x_i}\cos\varphi_{y_i} & 0 & 0 & 0 & 0 & 0 & 0 \\ 0 & \cos\varphi_{y_i} & -\sin\varphi_{y_i} & 0 & 0 & 0 & 0 & 0 & 0 \\ \sin\varphi_{x_i} & \cos\varphi_{x_i}\sin\varphi_{y_i} & \cos\varphi_{x_i}\cos\varphi_{y_i} & 0 & 0 & 0 & 0 & 0 & 0 \\ 0 & 0 & 0 & 1 & 0 & 0 & 0 & 0 & 0 \\ 0 & 0 & 0 & 0 & 1 & 0 & 0 & 0 & 0 \\ 0 & 0 & 0 & 0 & 0 & 1 & 0 & 0 & 0 \\ 0 & 0 & 0 & 0 & 0 & 0 & 1 & 0 & 0 \\ 0 & 0 & 0 & 0 & 0 & 0 & 0 & 1 & 0 \\ 0 & 0 & 0 & 0 & 0 & 0 & 0 & 0 & 1 \end{bmatrix}, \tag{1}$$

where φ_{x_i} and φ_{y_i} are the rotation angles in the *x*- and *y*-directions at the *i*-th node respectively. By multiplying the displacement and force vectors by this matrix, terms in Cartesian coordinates can be changed to those in a curved coordinate located along the neutral axes of a curved plate as

$$\left\{ \mathbf{u}_{\mathbf{n}} \quad \mathbf{w}_{\mathbf{n}} \quad \frac{\partial \mathbf{u}_{\mathbf{n}}}{\partial z} \quad \boldsymbol{\phi} \right\}^{\mathbf{T}} = \mathbf{T} \left\{ \mathbf{u} \quad \mathbf{w} \quad \frac{\partial \mathbf{u}}{\partial z} \quad \boldsymbol{\phi} \right\}^{\mathbf{T}}, \tag{2}$$

where $\mathbf{u}$, $\mathbf{w}$ and $\frac{\partial \mathbf{u}}{\partial z}$ are displacement vectors in the Cartesian coordinate and $\mathbf{u}_{\mathbf{n}}$, $\mathbf{w}_{\mathbf{n}}$ and $\frac{\partial \mathbf{u}_{\mathbf{n}}}{\partial z}$ are displacement vectors of the curved surface.

In order to check the established models, an impact hammer test was performed on a singly curved plate with a maximum rise of 20mm as shown in Figure 9 (a). The results of the measurement and FE analysis using MATLAB and Patran/Nastran are compared in Figure 9 (b). The model using MATLAB gives higher resonance frequencies than FE model (Quad4 elements used) using Patran/Nastran, especially for the lower modes. Although it gives such results, the pattern of mobility is similar in two models.

(a) (b)

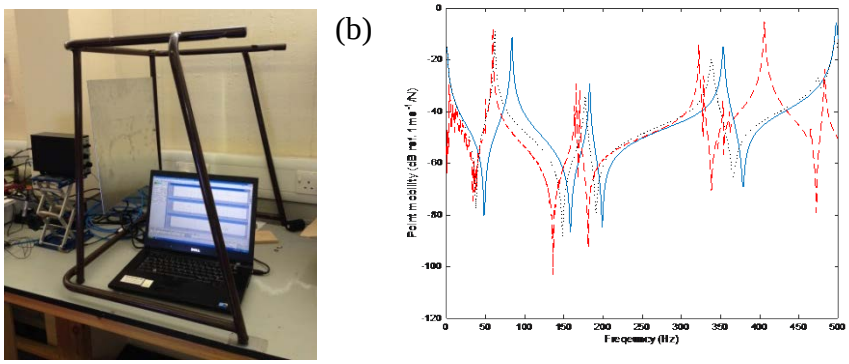

Figure 9: (a) Impact hammer test with a singly curved plate with maximum rise of 20mm and (b) Result comparison for an impact hammer test between an FE plate model and a real curved plate: —— FEM (MATLAB); - - - - Experiment; ------ FEM (Patran/Nastran)

Using these FE models of HAPCLD treatments and collocated error/control points at the centre, control gains and powers absorbed by PZT actuators were analysed as given in Table 1. In the case of collocation, since the locus of the Nyquist plot for the transfer function $H^{v}_{s} = H^{v}_{c}$ remain in the positive real half-plane, control is stable except for one case in Table 1. This can be explained through the study of the mode shapes in flat and curved plates. In spite of the symmetric motions of PZT patches around the centre of plates, the asymmetry of mode shapes at a certain mode can cause mismatch of motion which can cause the control to become unstable. Except for such cases, the control gain can be determined in one of two ways: the control gain which minimises the kinetic energy of whole structures, using

$$S_k(\omega) = \frac{\mathrm{M}}{2\mathrm{R}} \sum_{r=1}^{\mathrm{R}} \left| \tilde{v}_r(\omega) \right|^2, \tag{3}$$

where M is mass of the structure, R is the number of measurement points and $\left|\tilde{v}_r(\omega)\right|$ is the mean square value of the velocity measured by the *r*-th accelerometer; or, the gain which maximises the power absorbed by the PZT actuators,

$$S_p(\omega) = \frac{1}{2}\beta\left|\tilde{v}_c(\omega)\right|^2, \tag{4}$$

where β is the control gain and $\left|\tilde{v}_c(\omega)\right|$ denotes the mean square value of the control velocity. [6]

Table 1: Changes in control gain and maximum absorbed power for all cases according to the change in curvature

		Flat	10 mm	20 mm
Control gain	ACLD	1667.5	1795.5	1687.3
	APCLD	814.7	670.9	720.7
	AC/PCLD	192.7	41.7 (g_{3dB})	137.4
	AC/PSOLD	196.8	161.2	151.7
Absorbed power with optimised control gain (W)	ACLD	≈ 190	≈ 210	≈ 270
	APCLD	≈ 73	≈ 80	≈ 80
	AC/PCLD	≈ 18	≈ 12 (g_{3dB})	≈ 30
	AC/PSOLD	≈ 18	≈ 15	≈ 13

According to the analysis results, the reduction in mobilities were similar in spite of very different control gains and power absorbed. As seen in Table 1, AC/PSOLD treatment can give sufficient response reduction with smaller control gains and absorbed powers, and guarantee a stable and robust control results in any condition.

In order to validate this analytical result, transfer functions $H^f_{se} = H^f_{ce}$ and $H^v_s = H^v_c$ of each case were measured as shown in Figures 10 (a) and (b).

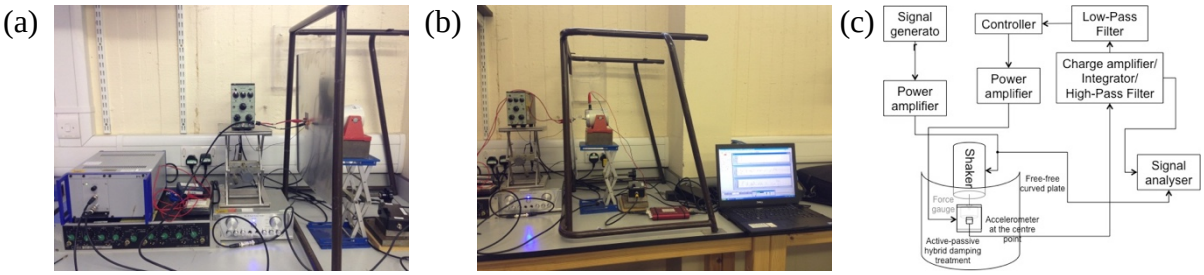

Figure 10: Input signal connection for (a) pseudo-random PZT excitation with electrical signal and (b) pseudo-random mechanical excitation by a shaker, and (c) Control scheme of whole system

With measured transfer functions, control simulations based on the block diagram of the control system were performed as shown in Figure 10 (c). The change of mobility of all configurations were measured and compared in Figure 11 (a). Although AC/PSOLD treatment did not give the largest reduction, the control gains which were determined with measured transfer functions should be considered. Since the control gains were easily affected by the experimental set-up, the ratio between mobility reductions and control gains should be considered as shown in Figure 11 (b). As can be noticed in Figure 11 (b), AC/PCLD and AC/PSOLD treatments can give similar reductions with the same control gain. However, as indicated by the analytical results, AC/PSOLD treatment is more robust than AC/PCLD treatment.

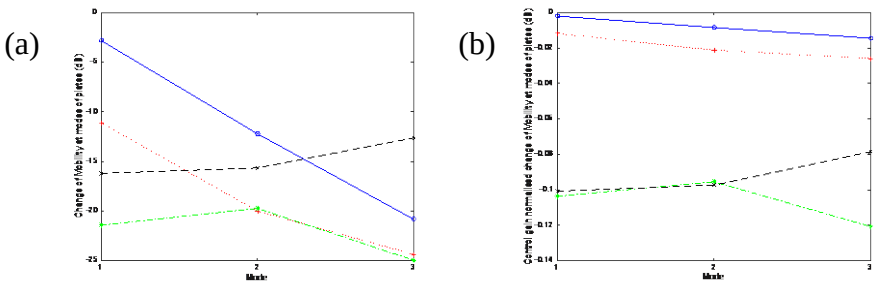

Figure 11: Change of Mobility by control of each HAPCLD treatment for curved plate with maximum rise of 20mm; —— ACLD (g_{3dB}: 1446.7), ------ APCLD (g_{3dB}: 943.48), - · - · AC/PCLD (g_{3dB}: 206.67) and – – AC/PSOLD (g_{3dB}: 160.74) (a) original values and (b) normalised values by the ratio of control gains with g_{3dB} of AC/PSOLD treatment

4. Conclusions

As can be seen from the simulation and experimental results, AC/PSOLD treatment can provide the largest reduction and most robust control of vibration of various structures of the four configurations of HAPCLD treatment. Through this series of studies, the conclusion in [1] was verified with measured data and confirmed to be valid for plates as well. When considering that curved plates are more common than beams in engineering applications, this result shows the benefits of AC/PSOLD treatment in vibration control. This can be extended to the control of radiated noise from structures such as car bodies and aircraft fuselages.

REFERENCES

1 Trindade, M. A. and Benjeddou, A., Hybrid Active-Passive Damping Treatments Using Viscoelastic and Piezoelectric Materials: Review and Assessment, *Journal of Vibration and Control*, **8** (6), 699-745, (2002).

2 Stanway, R., Rongong, J. A. and Sims, N. D., Active Constrained-Layer Damping: a State-of-the-art Review, *Proceedings of The Institution of Mechanical Engineers, Part I: Journal of Systems and Control Engineering*, **217** (6) , 437-456, (2003).

3 Koh, B., Rustighi, E., Mace, B. and Amabili, M, Numerical and Experimental Assessment of Hybrid Active-Passive Damping Treatments, *Proceedings of ISMA2012*, Leuven, Belgium, 17-19 September, (2012).

4 Koh, B., *Hybrid Active-Passive Constrained Layer Damping Treatments in Beams, Plates and Shells*, PhD Thesis, ISVR, University of Southampton, (2016).

5 Warburton, G.B., *The Dynamical Behaviour of Structures*, Pergamon Press Ltd., (1976).

6 Zilletti, M., *Self-Tuning Vibration Absorbers*, PhD Thesis, ISVR, University of Southampton, (2011).